Search for Glueballs*

Walter Toki

Department of Physics
Colorado State University
Ft. Collins, CO 80523

Abstract

In these Summer School lectures, we review the results of recent glueball searches. We begin with a brief review of glueball phenomenology and meson spectroscopy, including a discussion of resonance behavior. The results on the $f_0(1500)$ and $f_J(1700)$ resonances from proton-antiproton experiments and radiative J/ψ decays are discussed. Finally, $\pi\pi$ and $\eta\pi$ studies from D_s decays and exotic meson searches are reviewed.

*Work supported in part by the Department of Energy, contract DE-FG03-96ER40788.

1. Introduction

In this Summer School lecture, we review the search for glueballs. This topic is of great interest in light of more precise lattice QCD calculations on glueball masses and new data and glueball candidates from the LEAR groups.

The review begins with an introduction to glueball phenomenology in Chap. 2, a review of the $q\bar{q}$ meson model and predictions in Chap. 3, and a discussion of experimental spin-parity techniques in Chap. 4. The discussion of experimental results focuses on the search for scalar glueballs which decay into two pseudoscalar mesons. The main two candidates are the $f_0(1500)$ from $p\bar{p}$ experiments, discussed in Chap. 5, and the $f_J(1700)$ from radiative J/ψ decays, discussed in Chap. 6. New results from weak decays of charm D_s mesons are covered in Chap. 7, and the search for the exotic $\eta\pi$ resonance in Chap. 8.

Very recent material (August 1996) to be covered in the Topical Conference from LEAR (see M. Doser's talk[1]) and from BNL (see N. Cason's talk[2]) will not be discussed here.

Major references for this report include *the 6th International Conference on Hadron Spectroscopy* (Hadron '95) *Proceedings*,[3] J/ψ decays in *Physics Reports*,[4] "Review of Meson Spectroscopy,"[5] *Review of Particle Physics*,[6] *An Introduction to Quarks and Partons*,[7] and *Proceedings*[8] *of the Second Biennial Workshop on Nucleon-Antinucleon Physics*.

2. Glueballs

2.1 What Are Glueballs?

In the theory of Quantum Chromodynamics, gluons carry color charge, and consequently, gluons can interact with other gluons. This feature leads to couplings between two and three gluons. Hence, it may be possible for gluons to form bound states entirely composed of gluons with no quarks. These bound states of gluons are called glueballs.

We can form possible candidate glueball states by examining the states formed from combinations of gluons. Gluons are spin-one vectors and members of a color octet. To form color singlet mesons, the spin, space, and color symmetries must be properly combined. Two spin-one gluons in an S wave ($L = 0$) must be symmetric and will form states of $J^{PC} = 0^{++}$ or 2^{++}. The $L = 1$ case must have the antisymmetric $S = 1$ case and will yield $J^{PC} = 0^{-+}, 1^{-+}, 2^{-+}$. The different combinations are shown in Table 1.

L	J^{PC}
0	$0^{++}, 2^{++}$
1	$0^{-+}, 1^{-+}, 2^{-+}$
2	$2^{++}, 0^{++}, 4^{++}$
3	$2^{-+}, 3^{-+}, 4^{-+}$

Table 1. Possible spin-parity combinations for glueball states.

Several modes in the table are impossible to form from $q\bar{q}$ meson states. These are the $J^{PC} = 1^{-+}, 3^{-+}$ combinations. These states are called exotic or odd balls.

From Lattice QCD theory,[9] we expect the mass of the lowest lying glueball to be a scalar, $J^{PC} = 0^{++}$. The mass is expected to be in the 1-2 GeV/c^2 region. For a detailed discussion of mass predictions, see the lectures by T. DeGrand. The glueball width is not predicted by Lattice QCD theory. There are very rough ideas that the width should be in between the width of conventional mesons and OZI suppressed decays.

$$\Gamma_G = \sqrt{\Gamma_{OZI}\Gamma_{q\bar{q}}} = \sim \text{few 10's MeV}. \qquad \text{[Eq. 1]}$$

The width of an OZI suppressed ϕ decay is 4 MeV and the width of a typical OZI allowed meson decay of the rho meson is 150 MeV.

Since the glueball is a flavor singlet, the decay modes should be quite different from conventional mesons. A flavor singlet has zero isospin, and in the case of decays into two pseudoscalar mesons, the rates are set by the SU(3) Clebsch-Gordan coefficients coupling between a singlet and a pair of octet members. A scalar glueball candidate would be a meson that decays in an S wave into a pair of pseudoscalars such as $\pi\pi$, K_sK_s, K^+K^-, and $\eta\eta$.

A pure gluonic state should not contain charge; hence, there should be little coupling to photons. As a result, the glueball candidate should have no radiative decays such as a radiative transition or a two photon decay.

In conventional $q\bar{q}$ mesons, mixing is possible between states of the same J^{PC}, and such a situation may apply between glueballs and $q\bar{q}$ mesons. This possibility will complicate isolating a glueball. Hence, a careful understanding of conventional $q\bar{q}$ mesons will be necessary to interpret any glueball candidate. In addition, there is the possibility of hybrid states of a gluon plus quarks, $g + q\bar{q}$, which could also mask the search for glueballs.

In summary, the features of a glueball are:

- flavor symmetry in decay
- no radiative decays and no two photon decays
- mass 1-2 GeV (scalar glueball)
- decays into $\pi\pi$, K_sK_s, K^+K^-, and $\eta\eta$ (scalar glueball)
- a width of order of ~10's of MeV.

2.2 How Are Glueballs Produced?

Glueballs may be produced in reactions shown in Figure 1. The reactions include:

- radiative J/ψ decays
- OZI violating decay channels
- Pomeron exchange channels in central production.

Radiative J/ψ decays proceed via one photon and two gluons. The two gluons should couple to the glueball. Hence, scalar resonances produced in J/ψ decays are primary glueball candidates.

Charge exchange reactions such as $\pi^-p \rightarrow nX$, $X \rightarrow KK$, $\phi\phi$, or $K^-p \rightarrow \Lambda X$, $X \rightarrow \pi\pi$ are possible reactions for producing glueballs. In these reactions, the resonance X should be coupled by gluons to the other quark lines. These OZI violating decays can provide a very high statistics search from fixed-target experiments.

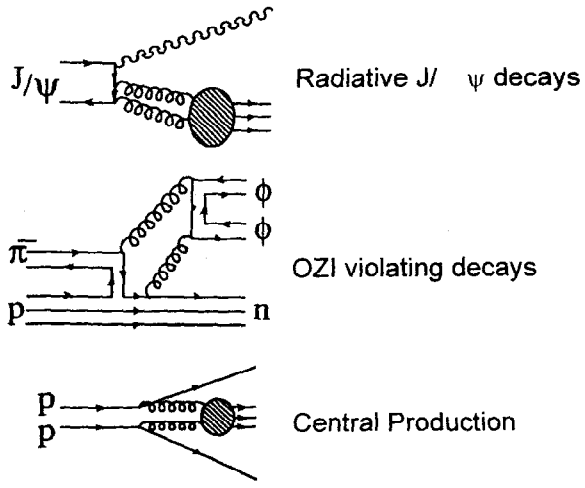

Figure 1. Gluon rich production reactions.

In high-energy reactions, peripheral collisions may be formed at small x_F. The proton-proton collisions may produce gluon collisions. This is called central production. The collision may also proceed via multiple gluons, and this is referred to as Pomeron exchange.

Other possible places for glueball production include nucleon-antinucleon annihilation. In this case, the quarks and antiquarks may rearrange themselves such that the final state produces multiple gluons plus a conventional $q\bar{q}$ meson. It is also possible that hybrid states and four quark states may be formed in this reaction as well.

Places where we DO NOT expect to produce glueballs are shown in Figure 2. These reactions include:

- two-photon production
- meson exchange.

Two-photon production of a meson is due to quark charges. Any state produced in two-photon production should be made up of quarks.

In meson exchange, the produced states should contain dominantly the quarks in the exchange. In the lower Figure 2, the mesons with hidden strangeness should be abundantly produced.

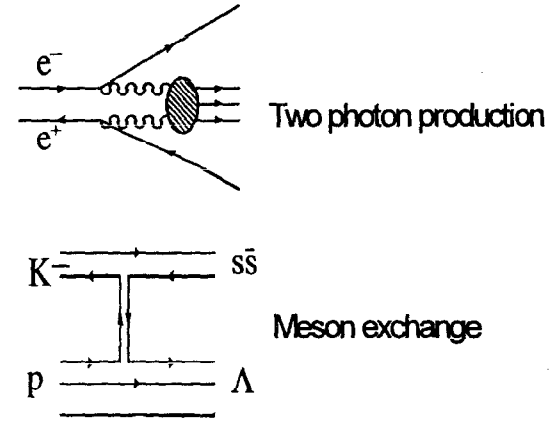

Figure 2. Reactions producing conventional $q\bar{q}$ mesons.

3. Quark-Antiquark Mesons

3.1 Review of Quark-Antiquark Mesons

The simple quark-antiquark model for mesons[10] is very successful in explaining virtually all meson properties, their quantum numbers, mass, and decay modes. In addition, there are few states that do not have a $q\bar{q}$ meson interpretation.

The properties of spin ½ quarks are listed in Table 2. Mesons are formed from quark q and antiquark $\bar{q}$ pairs. They form states similar to positronium like atoms with total spin S and angular spin L. The $q\bar{q}$ combination forms mesons with total spin $J = |L-S|, \ldots, |L+S|$. Since the quark and antiquark have opposite intrinsic parity, the meson parity depends on L and is $P = -(-1)^L$. For charge conjugation, only the neutral mesons can be eigenstates. If charge conjugation is applied to a neutral meson, the quarks switch to antiquarks and antiquarks to quarks. To form an eigenstate, the position and spins must be interchanged. The position interchange leads to a $(-1)^L$ dependence and the spin interchange leads to a $(-1)^{S+1}$ dependence. The combined operation yields a meson charge conjugation of $C = (-1)^{S+1}(-1)^L$. The flavor of the quark is defined to have the same sign as its charge.

Flavor	*u*	*d*	*s*	*c*	*b*	*t*
charge	+2/3	–1/3	-1/3	+2/3	–1/3	+2/3
I_3	+1/2	–1/2	0			
strangeness	0	0	–1			
charm				+1		
bottomness					–1	
topness						+1
mass (GeV)	0.3	0.3	0.5	1.5	5	160
spin	½	½	½	½	½	½
baryon number, *B*	1/3	1/3	1/3	1/3	1/3	1/3

Table 2. Quark properties with the constituent masses listed.

The quark and antiquark pair, when formed into special unitary (SU) multiplets, become mesons. A quark triplet of *u*, *d*, and *s* quarks, together with the corresponding antiquarks, form the SU(3) meson multiplets of an octet plus a singlet. These multiplets can be formed by constructing a triangle from the u, *d*, *s* triplet quarks on a plane with x and y axes of I_3 and hypercharge, $Y = (B+S)/2$, and an upside-down triangle of a triplet of antiquarks. Superimposing the triangle on the upside-down triangle leads to a six-sided octet on the I_3-Y plane. At the center of the diagram are two states, the eighth member of the octet and the singlet. In the quark model, these members can mix and the linear combinations are specified by an experimentally determined mixing angle. The mixed members of the SU(3) octet and singlet are the η and η' for the pseudoscalars and the ω and ϕ for the vectors.

If instead of a quark triplet we use a SU(4) quark quartet of *u, d, s, c* quarks and antiquarks, the SU(4) multiplets form a 16-plet. Using a similar scheme as in SU(3), the four quarks, *u, d, s, c* are plotted on a three-dimensional plot with variables, I_3-Y-C, forming a pyramid, and the antiquarks form an upside-down pyramid. Superimposing the center of the upside down pyramid on each corner of the pyramid leads to the 16-plet multiplet.

Table 3 lists the well-established mesons and their properties.

The simple quark model successfully explains

- meson mass splittings
- OZI allowed hadronic decays
- radiative and two photon decays.

Experimentally, every $q\bar{q}$ meson is accounted for except the light quark scalars! This may be related to some presently unknown reason that causes the scalar glueball to be experimentally hidden. We next discuss the scalar charmonium χ states and the experimentally known light quark scalars.

$N^{2S+1}L_J$	J^{PC}	I=1	I=0	I=0	I=0	I=1/2	I=1/2
1^1S_0	0^{-+}	π	η,η	η_c		K	D
1^3S_1	1^{--}	ρ	ω,ϕ	$J/\psi(1s)$	$\Upsilon(1s)$	$K^*(892)$	$D^*(2010)$
1^1P_1	1^{+-}	$b_1(1235)$	$h_1(1170)$, $h_1(1380)$	$h_c(1P)$		K_{1B}	$D_1(2420)$
1^3P_0	0^{++}			$\chi_{c0}(1P)$	$\chi_{b0}(1P)$	$K^*_0(1430)$	
1^3P_1	1^{++}	$a_1(1260)$	$f_1(1285)$, $f_1(1510)$	$\chi_{c1}(1P)$	$\chi_{b1}(1P)$	K_{1A}	
1^3P_2	2^{++}	$a_2(1320)$	$f_2(1270)$, $f_2(1525)$	$\chi_{c2}(1P)$	$\chi_{b2}(1P)$	$K^*_2(1430)$	$D^*_2(2460)$
1^1D_2	2^{-+}	$\pi_2(1670)$				$K_2(1770)$	
1^3D_1	1^{--}	$\rho(1700)$	$\omega(1600)$	$\psi(3770)$		$K^*(1680)$	
1^3D_2	2^{--}					$K_2(1820)$	
1^3D_3	3^{--}	$\rho_3(1690)$	$\omega_3(1670)$, $\phi_3(1850)$			$K^*_3(1780)$	
1^3F_4	4^{++}	$a_4(2040)$	$f_4(2050)$, $f_4(2020)$			$K^*_4(2045)$	
2^1S_0	0^{-+}	$\pi(1300)$	$\eta(1295)$	$\eta_c(2s)$		$K(1460)$	
2^3S_1	1^{--}	$\rho(1450)$	$\omega(1420)$, $\phi(1680)$	$\psi(2s)$	$\Upsilon(2s)$	$K^*(1410)$	
2^3P_2	2^{++}		$f_2(1810)$, $f_2(2010)$		$\chi_{b2}(2P)$	$K^*_2(1980)$	
3^1S_0	0^{-+}	$\pi(1770)$	$\eta(1760)$			$K(1830)$	

Table 3. Meson table, from the Particle Data Group tables.

3.2 χ States

The charmonium χ states are the three P wave ($L = 1$, $J^{PC} = 0^{++}, 1^{++}, 2^{++}$) members of the charm and anticharm quark mesons. Their masses are 3415, 3510, and 3556 MeV. The mass splitting is small and the electromagnetic transition rates from the electric dipole radiation from spin flip of the $\psi(3680)$ are predicted by theory and agree quite well with experimental measurements. The charmonium scalar is very well-understood, and we have no reason to expect mysterious behavior in the scalar P wave quark-antiquark states.

3.3 Scalar Mesons

If we now turn to the light quark scalar members, we find they are not listed in Table 3. The experimentally well-established scalars are the isovector, $a_o(980)$, and the isoscalars, $f_o(980)$ and $f_o(1370)$. The $f_o(980)$ predominantly decays into pion and kaon pairs, and the isovector, $a_o(980)$ into $\eta\pi$. The $f_o(1370)$ appears as a phase shift in S wave $\pi\pi$. These states were discovered 20 years ago. These states were formerly thought to be the light quark scalars, but recently this interpretation has been removed by the Particle Data Group. There are several reasons to suspect that these states are not the light $q\bar{q}$ scalar mesons. The mass splitting from the other light quark P wave states, $a_1(1260)$ and $a_2(1320)$, is very large. The real $q\bar{q}$ scalar should be close to these other P wave states. The $a_o(980)$ and $f_o(980)$ masses are at $K\bar{K}$ threshold. There has been a suggestion that these states are really $K\bar{K}$ molecules.[11] If in fact these presently known scalars are not the real $q\bar{q}$ scalars, we have two puzzles; namely, where are the real $q\bar{q}$ scalars and the glueball scalar?

3.4 What Is a Resonance?

What is a resonance? Most experimentalists look for peaks in invariant mass plots. However, many resonances are short-lived ($\tau \sim 10^{-24}$ sec.) and can have very large widths.

A resonance[12] is properly defined in terms of a phase shift. In classical electromagnetic theory,[13] if plane waves are incident on a metal or dielectric surface, the spherical scattered waves will get a phase shift that depends on the boundary conditions. In Quantum Mechanics, we consider plane waves incident on a target particle. A general solution from the Schrodinger Wave Equation will have the form $u_i(r,\theta,\phi) = e^{ikz} + e^{ikr} f(\theta,\phi)/r$, where

$$f(\theta) = \frac{1}{k}\sum_{l=0}^{\infty}(2l+1)T_l(E)P_l(\cos\theta). \qquad \text{[Eq. 2]}$$

We can rewrite T_l, the scattering amplitude, as

$$T_l(E) = \frac{\rho_l e^{2i\delta_l} - 1}{2i}, \qquad \text{[Eq. 3]}$$

where ρ_l and δ_l depend on the energy E. Using the cross section relation, we can obtain

$$\sigma(total) - \sigma(elastic\ scattering) = \frac{\pi}{k^2}\sum_{l=0}^{\infty}(2l+1)\left(1-\rho_l^2\right). \qquad \text{[Eq. 4]}$$

Thus, if $\rho_l = 1$, then the scattering is elastic and

$$T_l(E) = e^{i\delta_l}\sin\delta_l = \frac{1}{\cot\delta_l - i}, \qquad \text{[Eq. 5]}$$

then the cross section for the elastic case becomes

$$\sigma(a+b\to a+b;\text{elastic}) = \frac{\pi}{k^2}\sum_{l=0}^{\infty}(2l+1)\sin^2\delta_l. \qquad \text{[Eq. 6]}$$

The cross section reaches a maximum when δ_l goes to 90^0. For elastic scattering, $\rho_l = 1$, then

$$T_l = \frac{e^{2i\delta_l} - 1}{2i} = \frac{i}{2} + \frac{1}{2}\left(\sin 2\delta_l - i\cos 2\delta_l\right). \qquad \text{[Eq. 7]}$$

The plot of the real versus imaginary values of T_l is called an Argand diagram. This is shown in Figure 3 for the elastic case.

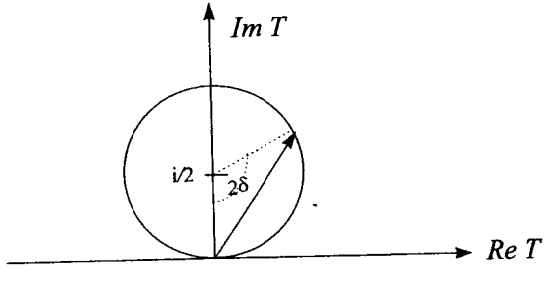

Figure 3. Argand diagram for elastic scattering.

If $\rho_l < 1$, for inelastic scattering, we have Figure 4 which simplifies to,

$$T_l = \frac{\rho_l e^{2i\delta_l} - 1}{2i} = \rho_l\left[\frac{e^{2i\delta_l} - 1}{2i}\right] + \frac{\rho_l - 1}{2i}. \qquad \text{[Eq. 8]}$$

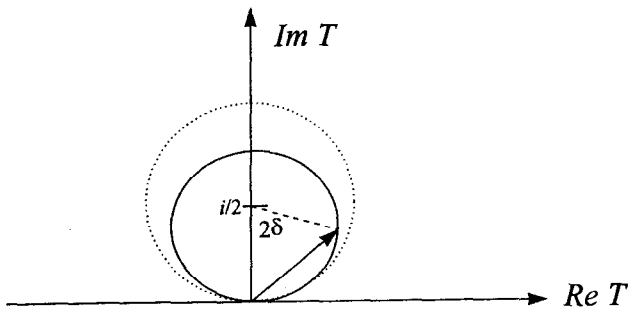

Figure 4. Argand diagram for inelastic scattering.

What is the connection with the Breit-Wigner form of a resonance in a mass plot? Since $T_l = 1/[\cot\delta_l - i]$ and the resonance is at $\delta_l(E_R) = 90°$, we have $\cos(\delta_l(E_R)) = 0$. We can expand the cotangent as

$$\cot(\delta_l(E)) \cong \cot[\delta_l(E_R)] + (E_R - E)\left.\frac{d\cot(\delta_l(E))}{dE}\right|_{E=E_R} + \ldots \qquad \text{[Eq. 9]}$$

$$\cot(\delta_l(E)) \cong (E_R - E)\left.\frac{d\cot(\delta_l(E))}{dE}\right|_{E=E_R} = (E_R - E)\frac{2}{\Gamma}.$$

Then, $T = [\Gamma/2]/[(E_R\text{-}E) + i\Gamma/2\ ]$. Figure 5 shows the scattering cross section versus the center-of-mass energy for a resonance. The half width, where the distribution falls to half its maximum, occurs at $E = E_R \pm \Gamma/2$.

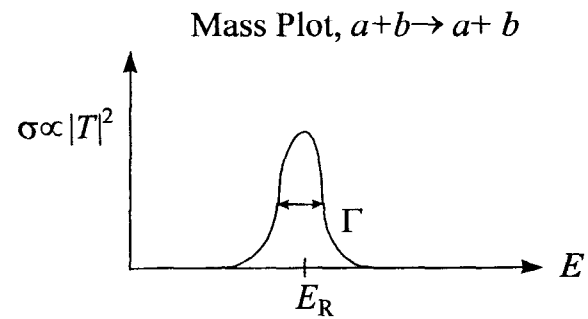

Figure 5. Mass plot and resonance width.

To determine a resonance, a δ_l phase shift of 180 degrees is required and the mass peak occurs at 90^0. To measure this phase shift in a particle physics experiment will require the phase shift to be measured *relative* to another partial wave. This is possible if there are other nearby resonances decaying into the same final state and whose Breit-Wigner shapes are already well-known.

There are cases where the resonance is very close to threshold,[14] such as the $f_o(980)$, and it is possible to have decays into $\pi\pi$ and $K\bar{K}$ In the case of the f_o, the mass is centered well above $\pi\pi$ threshold but for the decays into $K\bar{K}$, the mass is at $K\bar{K}$ threshold. In this case, unitarity and analyticity are used to extrapolate the $K\bar{K}$ threshold. The mass dependence is given in Eq. (10),

$$\frac{d\sigma}{dm} \propto \left| \frac{m_R\sqrt{\Gamma_o\Gamma_i}}{m_R^2 - m^2 - im_R(\Gamma_{\pi\pi} + \Gamma_{K\bar{K}})} \right|^2 \qquad \text{[Eq. 10]}$$

$$\Gamma_{\pi\pi} \propto g_\pi p$$

$$\Gamma_{K\bar{K}} \propto g_K\sqrt{m^2/4 - m_K^2}, \text{ above } K\bar{K} \text{ threshold}$$

$$\Gamma_{K\bar{K}} \propto ig_K\sqrt{m_K^2 - m^2/4}, \text{ below } K\bar{K} \text{ threshold}.$$

Above $K\bar{K}$ threshold, the $\pi\pi$ mass shape is depressed by rapidly increasing $\Gamma_{K\bar{K}}$, and below threshold, the $\pi\pi$ mass shape is depressed if g_K is large. This effect of

this width dependence near threshold is seen in the decay of $J/\psi \rightarrow \phi f_o(980)$, $f_o(980) \rightarrow K\overline{K}$, $\pi\pi$ in Figure 6. In the $\pi\pi$ decay mode, the Breit-Wigner shape of the $f_o(980)$ is cut short as the $\Gamma_{K\overline{K}}$ threshold opens up and the denominator in $d\sigma/dm$ increases. For the $K\overline{K}$ decay mode, the shape of $d\sigma/dm$ can be obtained using the $\Gamma_{K\overline{K}}$ below threshold.

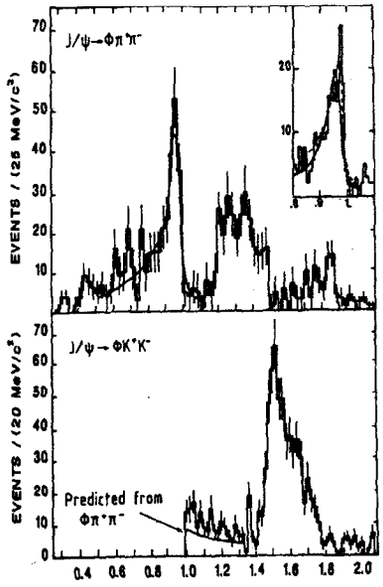

Figure 6. Mass plots of $\pi^+\pi^-$ from $J/\psi \rightarrow \phi\pi\pi$ and K^+K^- from $J/\psi \rightarrow \phi KK$. Results from the DM2 experiment.[4]

Threshold effects can create seemingly narrow peaks, as in the $f_o(980) \rightarrow \pi\pi$ case. This can occur any place near the threshold of the final secondary particles. For example, below are listed places were several peaks can occur due to threshold effects of a resonance. There are numerous such places and corresponding candidates.

- $K\overline{K}$ (~1 GeV); candidates, $f_o(980) \rightarrow \pi\pi$, $a_o(980) \rightarrow \eta\pi$
- $K^*\overline{K}$ (~1.4 GeV); candidates, $f_1(1420)$, $\eta(1440) \rightarrow K\overline{K}\pi$
- $\rho\rho$, $\omega\omega$ (~1.5 GeV); candidates, $f_o(1500) \rightarrow \pi\pi$
- $K^*\overline{K}^*$ (~1.8 GeV); candidates, $f_J(1710) \rightarrow K\overline{K}$
- $p\overline{p}$ (~2 GeV); candidates?
- $\Lambda\overline{\Lambda}$ (~2.23 GeV); candidates, $\xi(2230) \rightarrow K\overline{K}$.

4. Experimental Techniques

4.1 Spin-Parity Determination

Spin-parity determination can be understood fairly simply by using the helicity formalism[15] for two body decays. Decays with more than two secondaries can be extended by considering the decay in terms of sequential two body decays. If a particle X decays into particles a and b (see Fig. 7), the amplitude for the decay into two pseudoscalars is as follows:

$$\text{amplitude} \sim Y_{lm}(\theta,\phi). \qquad \text{[Eq. 11]}$$

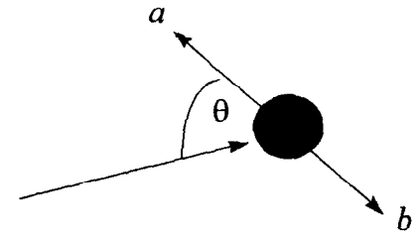

Figure 7. Decay angles of X decaying into a and b particles.

The amplitude for decay of a scalar X is simply $\sim Y_{00}$, which is constant. The amplitude for decay of a spin two-particle X is $\sim\Sigma\, a_m\, Y_{2m}(\theta,\phi)$, where the a_m are coefficients that depend on the magnitude of the different helicity states m. It is

possible to fit the distribution of decay angles θ and ϕ, and to find which Y_{lm} choice fits the best in order to determine the spin. If the particle has spin 2, we will need to fit the unknown helicity amplitudes a_m. Usually, they will become additional unknown parameters to fit.

A more sophisticated approach utilizes moments. The idea is to weight each event by Y_{lm}'s. Suppose an amplitude is given by $A = \sum a_{Jmm'} D^{J}_{mm'}(\Omega)$. Then the intensity in the amplitude is squared,

$$|A|^2 = \sum a_{Jm_1m_1'} D^{J}_{m_1m_1'}(W) \sum a^*_{Jm_2m_2'} D^{J*}_{m_2m_2'}(W). \qquad \text{[Eq. 12]}$$

The pair of D functions can be equated to a single D function using a summation relation,

$$D^{J_1}_{m_1m_1'}(\Omega) D^{J_2}_{m_2m_2'}(\Omega) = \sum_{J_3=|J_1-J_2|}^{J_1+J_2} \langle J_1m_1, J_2m_2 | J_3m_3 \rangle \langle J_1m_1', J_2m_2' | J_3m_3' \rangle D^{J_3}_{m_3m_3'}(\Omega). \qquad \text{[Eq. 13]}$$

Using this relation, the intensity $|A|^2$, can be written as a sum of a single D function.

$$|A|^2 = \sum_{J=|J_1-J_2|}^{J_1+J_2} T_{Jmm'} D^{J}_{mm'}(\Omega). \qquad \text{[Eq. 14]}$$

Now the coefficient $T_{Jmm'}$, is a complicated complex coefficient that is a sum of products of $a_{Jmm'}$. Also, although we have the intensity as a linear combination of a single D functions, the value of J will vary from $|J_1-J_2|$ to J_1+J_2. So to study spin 2 will require a J value of up to four. Since the intensity can be written as a sum of single D's, we can extract the value of the coefficient $T_{Jmm'}$ by weighting the data events by a particular $D^{*J_1}_{m_2m_3}(\Omega)$, which will project out the coefficient $T_{J_1m_2m_3}$. The other coefficients are associated with orthogonal D functions and will not contribute. This result assumes that the efficiency is uniform in angle. If the efficiency is not uniform, the coefficients can still be determined by a slightly more complicated correction procedure.

Once we obtain all the values of the coefficients, $T_{Jmm'}$, we can then invert the process to obtain the values of the $a_{Jmm'}$. In some cases, the inversion can have ambiguities.

4.2 Dalitz Plot Analysis

In spin-parity analyses of states that decay into three mesons, the study of the Dalitz plot has provided important information. If a particle X decays into mesons, a, b, and c, $X \rightarrow a + b + c$, it is possible that intermediate states are formed between any two of the three particles. For example, the reaction $J/\psi \rightarrow \rho\pi \rightarrow \pi^+\pi^-\pi^0$, has an intermediate state, $\rho \rightarrow \pi\pi$. These intermediate states can be studied with the use of the Dalitz plot. In a Dalitz plot, the invariant mass squared of two of the particles is plotted versus the invariant mass squared of a second pair of the particles (at least one particle is common to the two pairs). A schematic Dalitz plot is shown in Figure 8 with bands created by two-body resonances. Figure 9 is a Dalitz plot of the $\pi^+\pi^0$ mass squared versus the $\pi^-\pi^0$ mass squared.

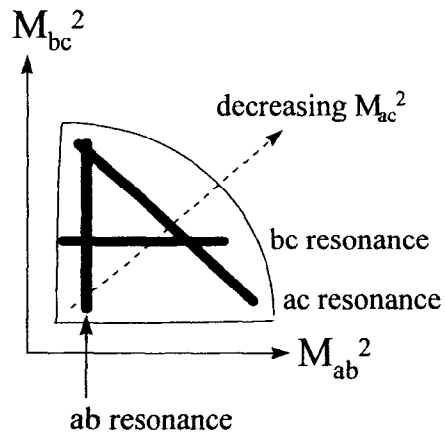

Figure 8. Schematic diagram of a Dalitz plot.

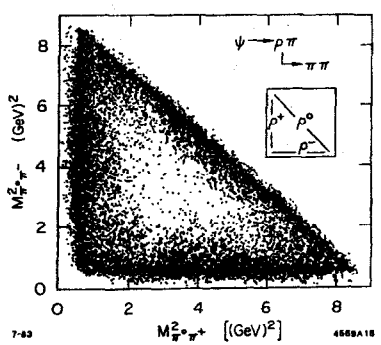

Figure 9. Dalitz plot of $J/\psi \to \rho\pi \to \pi^+\pi^-\pi^0$, from Mark III.[4]

The concentration of events on the vertical band corresponds to $\rho^+ \to \pi^+\pi^0$, the horizontal bank corresponds to $\rho^- \to \pi^-\pi^0$, and the diagonal band corresponds to $\rho^0 \to \pi^+\pi^-$. The density of the events along the line depends upon the spin of the intermediate particle. In this case, the ρ has spin one and the density peaks at the middle of the band and drops to zero at the ends of the band. If the two body resonance has spin zero, the band will have a uniform distribution.

The spin of a particle that decays into three mesons can be determined by trying different spin-parity hypotheses and comparing the probability for each hypothesis.

4.3 K Matrix Formalism

The general idea of the K matrix formalism[16] is to include unitarity in a convenient manner. Suppose a resonance X decays into two bodies such as $\pi\pi$, KK, $\eta\eta$. We can write the unitarity requirement on the S matrix as $\Sigma|S_{ij}|^2 = 1$. If we use the transition matrix T, defined from the S matrix as $S = I + 2iT$, where I is the identity matrix, then unitarity is given by $Im\ T_{if} = \Sigma\, q_j\, T_{ji}^*\, T_{jf}$ where q_j is the momentum in the cms for channel j.

It turns out that imposing unitarity directly on the T matrix is not a convenient approach. Instead, we can redefine T in terms of another matrix called the K matrix via $T = K(I - iQK)^{-1}$, where $Q_{ij} = q_i\delta_{ij}$. With this definition, unitarity is automatically satisfied. This can be checked by substituting this equation into $Im\ T_{if} = \Sigma\, q_j\, T_{ji}^*\, T_{jf}$. Hence, a convenient method is to approximate T (or S) by representing T in terms of K. If time invariance holds, K will be real and symmetric. In older textbooks,[17] this matrix is also called the reaction or reactance matrix.

5. Proton-Antiproton Searches

In recent years, the most important new data on the search for glueballs and new hadronic states have come from the study of $p\bar{p}$ reactions at LEAR, and notably, the Crystal Barrel experiment with its very high statistics data. A scalar resonance at a mass of 1.5 GeV has been observed. It may have been seen in an earlier low statistics BNL experiment. In early LEAR runs, it was perhaps overlapping and

misidentified with a tensor meson called the AX. Later, after analysis of the very high statistics Crystal Barrel data, clear evidence for a scalar was obtained. Confirming evidence has not yet been obtained from the charmonium experiment E760 at FNAL. In this section, we discuss the $p\bar{p}$ results in historical order and discuss in detail the study of the resonance at a mass of 1500 MeV.

5.1 Early Results

The early results in $p\bar{p}$ physics are from BNL low statistics data studying the reaction, $p\bar{n} \rightarrow 2\pi^+\pi^-$. The results indicated a ρ and $f_2(1270)$ signal and a bump at 1527 MeV with a width of $\Gamma = 101$ MeV. This data is shown in Figure 10.

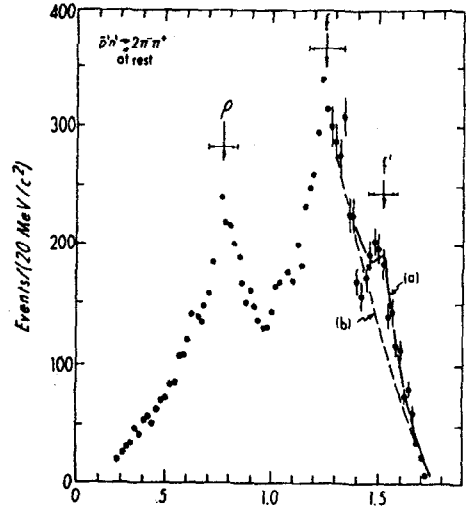

Figure 10. $\pi^+\pi^-$ mass from BNL.[18]

At LEAR, the ASTERIX experiment sent an antiproton beam into a gaseous H_2 target and observed a peak near 1500 MeV. The OBELIX experiment studied $\bar{n}p \rightarrow \pi^+\pi^+\pi^-$ in flight. The $\pi^+\pi^-$ mass plot is shown in Figure 11. The observed peak includes the ρ, the $f_2(1270)$, and a peak at ~1.5 GeV. This resonance was called the AX and the initial spin-parity studies suggested $J^{PC} = 2^{++}$.

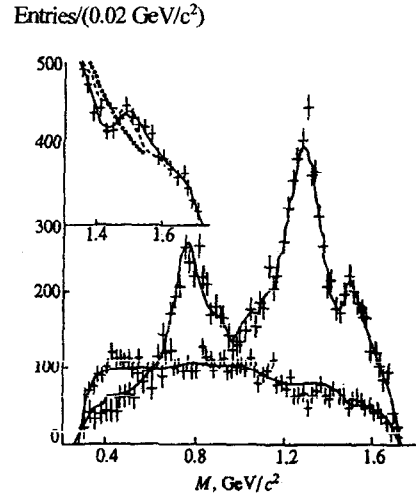

Figure 11. $\pi^+\pi^-$ mass results from the OBELIX experiment.[19]

GROUP	Channel	Mass	Width	BR (10^{-3})	J^{PC}
ASTERIX	$\pi^+\pi^-\pi^0$	1565 ± 20	170 ± 40	3.7 ± 0.6	2^{++}
CRYSTAL BARREL	$\pi^0\pi^0\pi^0$	1515 ± 10	120 ± 10	2.0 ± 0.6	2^{++}
OBELIX	$\pi^+\pi^-\pi^+$	1502 ± 9	130 ± 10	-	2^{++}
E760	$\pi^0\pi^0\pi^0$	1498 ± 4	141 ± 10	-	
BNL	$\pi^+\pi^-\pi^0$, $\pi^0\pi^0\pi^0$, $\pi^+\pi^-\pi^+$	1527 ± 5	101 ± 13	1.6 ± 0.5 2.6 ± 0.4	
Bridge *et al.*	$2\pi^+3\pi^-$ (ρρ)	1477 ± 5	116 ± 9	37 ± 0.3	2^{++}

Table 4. "AX" results.

5.2 High Statistics Crystal Barrel Results

The Crystal Barrel group published early results on $p\bar{p} \rightarrow \pi^0\pi^0\pi^0$ in May 1991 based on 55K events. This analysis obtained a spin parity result of $J^{PC} = 2^{++}$ for a resonance at a mass of 1515 MeV decaying into $\pi^0\pi^0$.

In December 1993, a complicated analysis simultaneously fit a resonance $X \rightarrow \pi^0\pi^0$ in the reaction $p\bar{p} \rightarrow \pi^0\pi^0\pi^0$, and $X \rightarrow \eta\eta$ in the reaction $p\bar{p} \rightarrow \eta\eta\pi^0$. This resulted in the first evidence for two separate scalar signals with masses and widths at $M = 1565$ MeV, $\Gamma = 268$ MeV and $M = 1520$ MeV, $\Gamma = 148$ MeV.

In January 1995, based on 712K events, the reaction on $p\bar{p} \rightarrow \pi^0\pi^0\pi^0$ was analyzed with an amplitude analysis utilizing the K matrix formalism. The amplitude fitted was

$$A\left[{}^{2S+1}L_J\right](p,q) = \sum_{L,l} Z\left[{}^{2S+1}L_J\right]_{,L,l}(p,q) B^L(p) F^l(q)$$

$$A\left[{}^{2S+1}L_J\right](p,q) = \sum_{L,l} Z\left[{}^{2S+1}L_J\right]_{,L,l}(p,q) B^L(p) F^l(q)$$

$F^l(q)$ are the dynamical functions containing the K matrix

$B^L(p)$ are the angular momentum barrier factors

$Z\left[{}^{2S+1}L_J\right]_{,L,l}$ are the Zemach spin parity functions

The sequential decay was set up as shown in Figure 12.

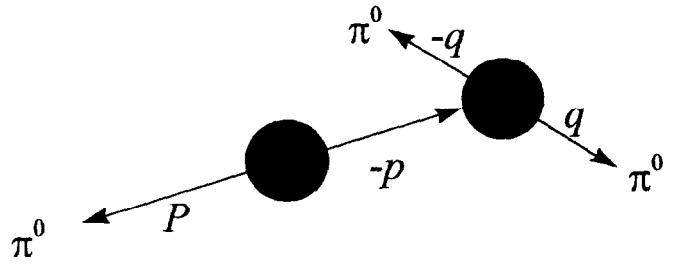

Figure 12. Decay chain of $p\bar{p} \rightarrow X \rightarrow \pi^0\pi^0$.

A total of 34 parameters are used to fit the Dalitz plot in 1338 nonzero cells. The K matrix poles are obtained, and then using the relation $T = (I - iKQ)^{-1}K$, the mass and width are obtained from the T matrix. The results of this fit are shown in Table 5.

Spin	Mass (MeV)	Γ (MeV)	*BR*	Comments
0	994 ± 5	26 ± 1	42%	old S^*
0	1330	760		old ε
0	1490 ± 13	120 ± 15	12%	new scalar
2	1285	195	29%	$f_2(1270)$
2	1520	135	17%	old AX

Table 5. Results for T matrix poles in Crystal Barrel data.

In the high statistics Dalitz plot in Figure 13, we can observe several features:

- a flat band at M~1500 MeV
- a high spin at M~1540 MeV
- a dip at the $f_0(980)$
- a peak in the $f_2(1270)$ mass region.

There is clear evidence for a scalar at 1500 MeV. The K matrix analysis reveals a scalar with a mass of 1490 MeV and a broad scalar at 1330 MeV which may be the old ε scalar. The tensors $f_2(1270)$ and the AX at 1520 MeV are also obtained.

The Crystal Barrel group also studied the decay $p\bar{p} \rightarrow \pi^0\eta\eta$. The Dalitz plots are shown in Figure 14 and Figure 15. A couple of features are apparent:

- a $\delta^0 \rightarrow \eta\pi^0$ signal
- an $\eta\eta$ resonance in the 1.3–1.5 GeV mass region.

Utilizing the K matrix formalism, similar results of a scalar at 1360 MeV and 1500 MeV are obtained for the $\eta\eta$ channel.

The decay modes of the $f_o(1500)$ are listed in Table 6. The upper limit in the $K\bar{K}$ mode is obtained from old BNL results.

Decay Mode X	Branching Fraction of f_o
$\pi^0\pi^0$, $\pi^+\pi^-$	$[38 \pm 10] \times 10^{-4}$
$\eta\eta$	$[6.2 \pm 2.8] \times 10^{-4}$
$\eta'\eta$	$[1.5 \pm 0.5] \times 10^{-4}$
$4\pi^0$	$3.4 \times [3.8 \pm 10] \times 10^{-4}$
$K\bar{K}$	$< [5\text{-}6] \times 10^{-4}$ (from Gray *et al.*[18])

Table 6. Product branching fractions $B(p\bar{p} \rightarrow \pi^0 f_o) \times B(f_o \rightarrow X)$.

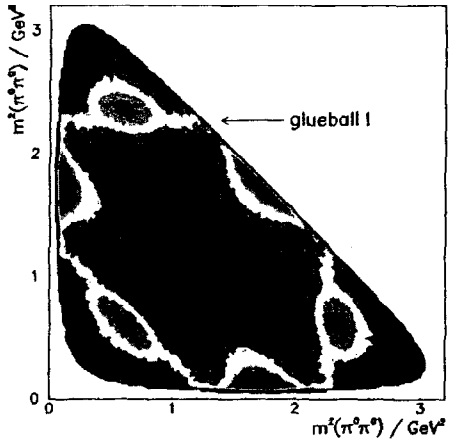

Figure 13. Dalitz plot for $p\bar{p} \rightarrow \pi^0\pi^0\pi^0$ from the Crystal Barrel.[20]

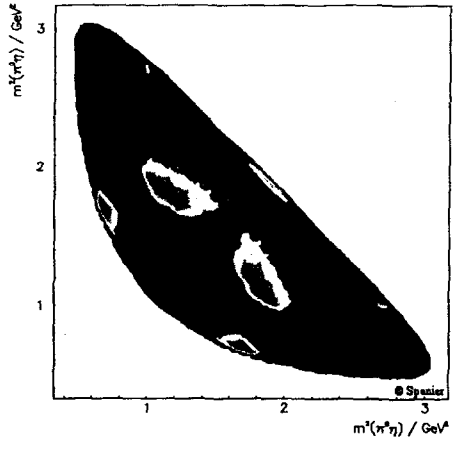

Figure 14. Dalitz plot for $p\bar{p} \rightarrow \eta\pi^0\pi^0$ from the Crystal Barrel.[21]

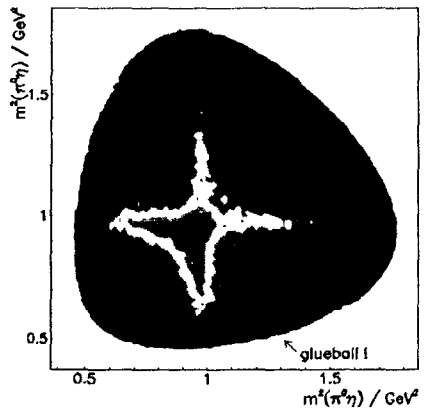

Figure 15. Dalitz plot for $p\bar{p} \to \eta\eta\pi^0$ from the Crystal Barrel.

5.3 E760 Results

The E760 experiment at FNAL collides antiprotons on a proton gas jet target at center-of-mass energies of 2.98 and 3.526 GeV to study charmonium states. The group has studied the $3\pi^0$ and $\pi^0\eta\eta$ decays. The Dalitz plots from E760 are shown in Figure 16 and Figure 17. We can see the following:

- in $3\pi^0$, there are $2\pi^0$ peaks at 1270, 1500, and 2000 MeV
- in $\pi^0\eta\eta$, there are $\pi^0\eta$ peaks at 980 and 1320 MeV
- in $\pi^0\eta\eta$, there are $\eta\eta$ peaks at 1500 and 2100 MeV.

Since the center-of-mass energy is higher than for Crystal Barrel, the resonances seen by E760 are not caused by reflections on the Dalitz plot. Since the center-of-mass energy is different, perhaps the production rate of the $f_0(1500)$ and the AX(1520) is different, so they may not be able to confirm the existence of the scalar. A spin-parity determination has not yet been published by the E760 group. However, a fit to the $\pi\pi$ mass plot has been performed including seven resonances and is shown in Figure 18.

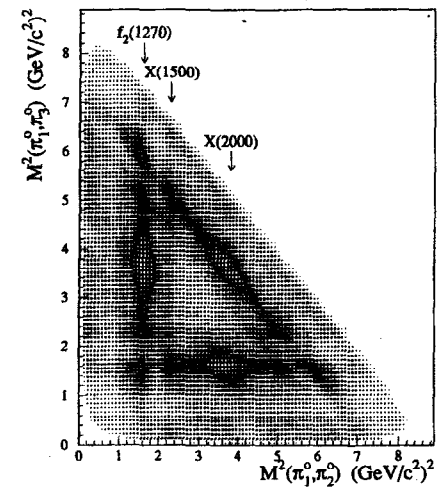

Figure 16. Dalitz plot for $p\bar{p} \to \pi^0\pi^0\pi^0$ from E760 (Ref. 22).

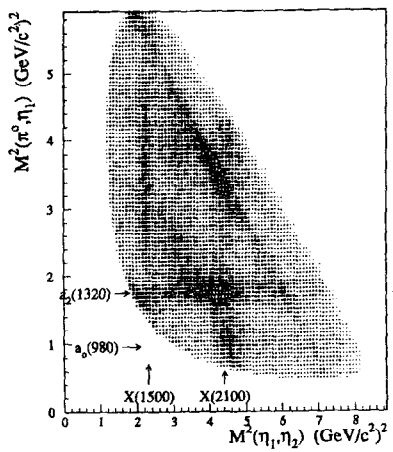

Figure 17. Dalitz plot for $p\bar{p} \rightarrow \eta\eta\pi^0$ from E760.

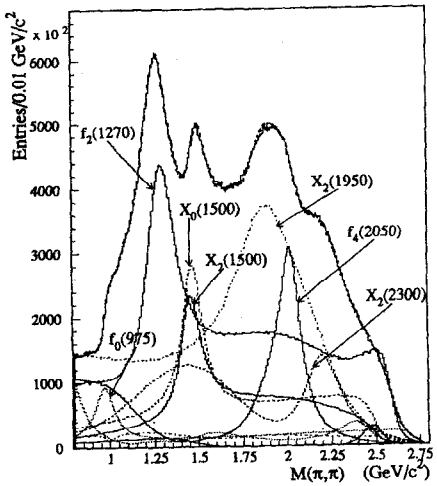

Figure 18. Fit to the $\pi\pi$ mass spectrum from E760.

5.4 Other Developments

A very important question is: Does the $f_0(1500)$ appear in radiative J/ψ decays? In the radiative decays into four pions from the DM2 group, a peak appears near 1500 MeV as shown in Figure 19.

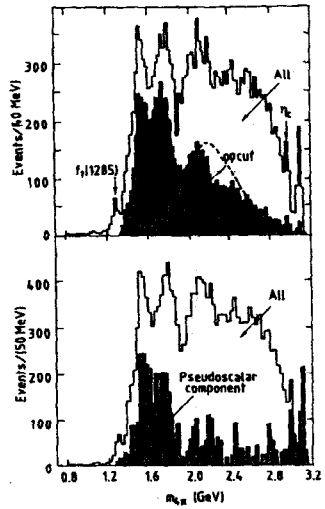

Figure 19. $J/\psi \rightarrow \gamma 4\pi$ from the DM2 group.[23]

D. Bugg *et al.*,[24] have analyzed the $J/\psi \rightarrow \gamma 4\pi$ channel from the Mark III group. The Mark III four pion mass distribution, however, does look different from the DM2 data and there is no visible peak at 1500 MeV. Using a four body partial wave analysis and assuming that the pion pairs form scalars, they conclude there is evidence for a scalar near 1500 MeV. In Figure 20, the left plot is the fit result including the $f_0(1500)$ and right plot is the fit result not including the $f_0(1500)$. In Figure 21, the lower left and right plots are the scalar and tensor intensities. The scalar intensity is fit with resonances at 1505, 1750, and 2104 MeV.

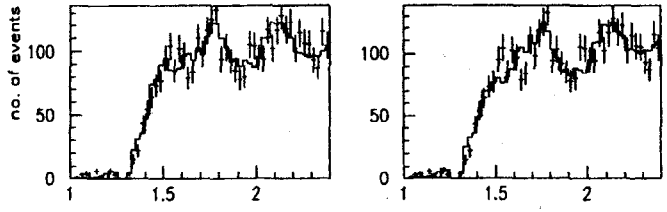

Figure 20. Mass plot fits to the Mark III data.

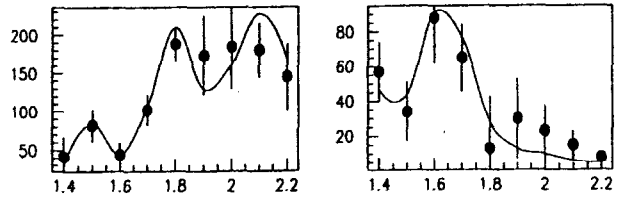

Figure 21. Partial wave analysis of Mark III data.[24]

From the Bugg *et al.* analysis, the branching ratio the $B(J/\psi \rightarrow \gamma f_0(1500) \rightarrow \pi\pi) = 5.7 \times 10^{-4}$ is obtained. Using a Crystal Barrel branching ratio of $B(f_0 \rightarrow 4\pi)/B(f_0 \rightarrow 2\pi) = 3.4 \pm 0.8$, we can compare the rate to the $f_2(1270)$ and find that the radiative J/ψ decays have a rate of $f_0 \rightarrow \pi\pi$ that is 15% of the $f_2(1270)$. If we look at the Crystal Ball results on $J/\psi \rightarrow \gamma\pi^0\pi^0$ in Figure 22, we observe a clear $f_2(1270)$ signal. At 1500 MeV, there is a dip where we would expect the f_0 signal that is 15% of the neighboring $f_2(1270)$ signal. There is a peak of 14 events at 1450 MeV which appears below the $f_0(1500)$.

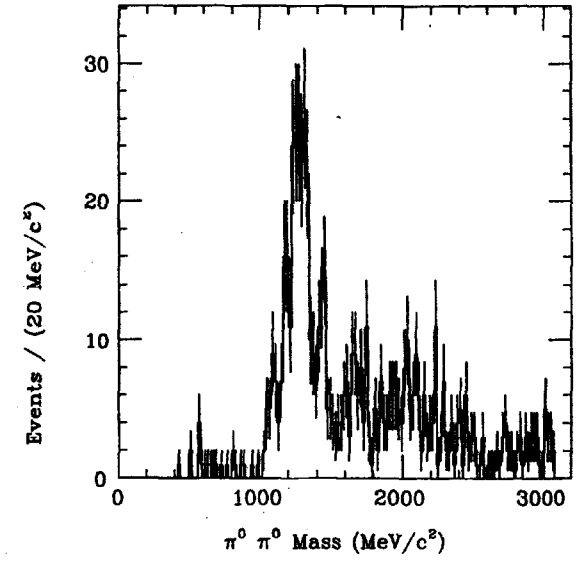

Figure 22. $J/\psi \rightarrow \gamma\pi^0\pi^0$ from the Crystal Ball.[25]

5.5 Discussion of $f_0(1500)$

The $f_0(1500)$ results are summarized below:

- mass ~1500 MeV
- width ~120 MeV
- decays to $\pi^0\pi^0$, 4π, $\eta\eta$, $\eta\eta'$ (possibly related to the GAMS resonance at 1590 MeV)
- does not decay to $K\bar{K}$
- $J^{PC}=0^{++}$, a 2^{++} resonance is nearby
- produced in $p\bar{p}$,

not seen in:

- two photon, fixed-target $\pi\pi$ scattering, central production.
- J/ψ evidence in 4π, but 2π may be controversial?

Possible interpretations of this state include glueball, threshold effect, four quark state, and antinucleon-nucleon bound state.

In a glueball interpretation, f_0 is a strong candidate. The main puzzles, however, are the lack of SU(3) flavor singlet symmetry[26] and the lack of any large $\pi\pi$ signal in radiative J/ψ decays. It is possible that mixing may be suppressing the $K\bar{K}$ mode; however, none of the radiative J/ψ results show any hint of a $\pi\pi$ signal at 1.5 GeV.

The $f_0(1500)$ mass is near the $\omega\omega$ and $\rho\rho$ thresholds. This may be accidental or may support evidence that it is a molecule or a threshold effect, although there is little evidence for direct $\omega\omega$ or $\rho\rho$ decay.

Since the f_0 is seen in $p\bar{p}$ annihilation, there should be many up and down quarks available to form four-quark states. If four-quark states are being formed, there may be $I = 0$ and possibly $I = 2$ states. As a long shot, we took a brief look for charge two pion pairs in Figure 23, but no evidence for a mass bump in double charged pion pairs is seen.

Another interpretation[27] has been put forward that the f_0 is a quasi nuclear antinucleon-nucleon bound state. In this model, $p\bar{p}$ annihilation radiates a π to form a lower mass bound state, which is below $p\bar{p}$ threshold and decays into two pions. This model predicts both scalar and tensor states.

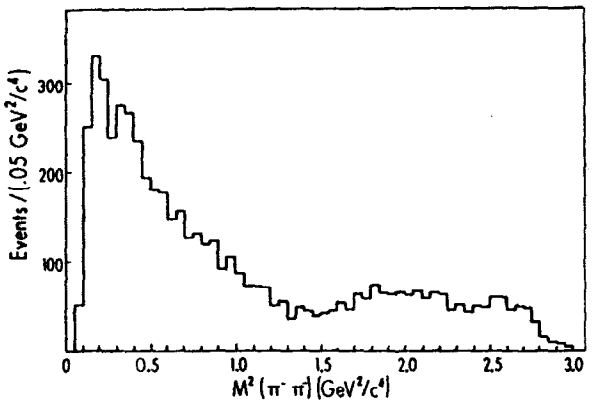

Figure 23. $M^2(\pi^-\pi^-)$ distribution from BNL.[28]

6. $f_J(1700)$ Resonance

The $f_J(1700)$ resonance was first observed in radiative J/ψ decays into K^+K^- and K_sK_s. Early spin-parity tests suggested spin two, but recently spin zero has been obtained. The $f_J(1700)$ may also be seen in central production, although the analysis suggests spin two. Here we discuss the early observations in radiative J/ψ decays, the fixed-target experiments, and finally, the spin parity tests.

6.1 J/ψ Radiative Decays

The first evidence for a new resonance in radiative J/ψ decays into two pseudoscalars came from Mark II[29] studying $J/\psi \rightarrow \gamma KK$. The KK mass plot is shown in Figure 24. The Mark II mass was m = 1708 ± 30 MeV.

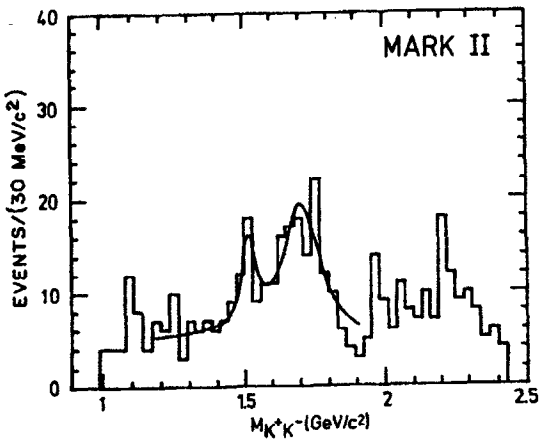

Figure 24. KK mass distribution from $J/\psi \rightarrow \gamma KK$ from Mark II.[29]

Soon afterwards, the Crystal Ball group[30] observed an $\eta\eta$ signal at $m = 1670 \pm 50$ MeV in $J/\psi \rightarrow \gamma\eta\eta$. A spin-parity analysis provided evidence for spin two. The mass and fit to the decay angles are shown in Figure 25.

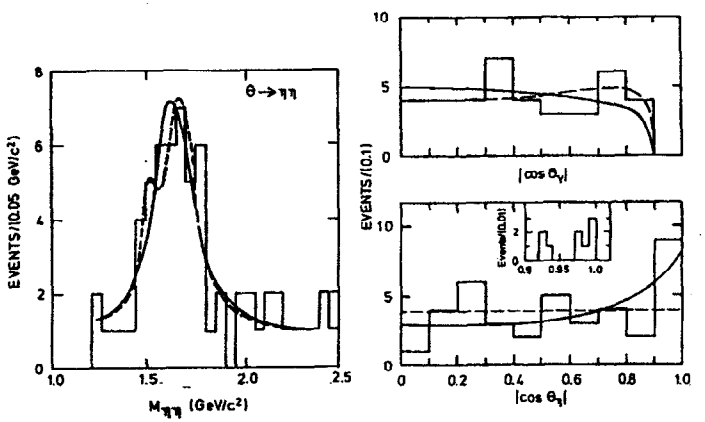

Figure 25. $\eta\eta$ mass distribution from $J/\psi \rightarrow \gamma\eta\eta$, from the Crystal Ball.[30]

Later, the Mark III and DM2 group observed with higher statistics this signal in radiative J/ψ decays in the K^+K^- and K_sK_s modes. The plots from the Mark III for the KK and $\pi\pi$ radiative decays are shown in the upper plots in Figure 26. In the radiative J/ψ decays, there is some evidence in the $\pi\pi$ mode for the $f_J(1700)$, but there is no evidence for the $f_0(980)$. In the hadronic decays of $J/\psi \rightarrow \phi+X$, we observe the $f_0(980)$ and $f_2(1500)$. And in the hadronic decays of $J/\psi \rightarrow \omega+X$, we observe the $f_2(1270)$ and an enhancement in the KK channel in the 1700 MeV mass region.

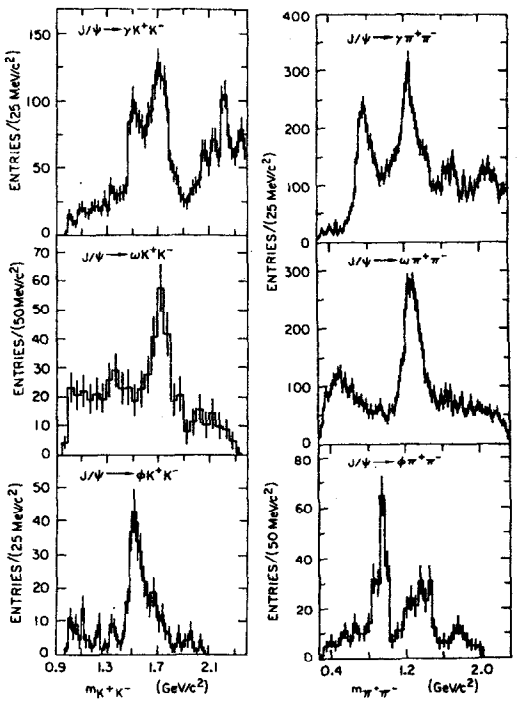

Figure 26. Mass distributions from $J/\psi \rightarrow KK + [\gamma, \omega, \phi]$, $\pi\pi + [\gamma, \omega, \phi]$ from Mark III.

In the Mark III data,[31] a simple maximum likelihood fit was applied to the events in the 1700 MeV region, and it was determined that it was more likely that all the events in that region were spin two instead of all spin zero. This primitive analysis did not allow for overlapping resonances but only all spin zero or all spin two in the mass region.

6.2 *Fixed-Target Results*

In fixed-target experiments, there is a mixture of evidence for a resonance decaying into two pseudoscalars in the 1700 MeV mass region. The LASS group studied the reaction $K^- p \rightarrow KK\Lambda$. In Figure 27 is shown the $K_S K_S$ mass plots from the radiative J/ψ decays and the $K^- p$ reaction. Here, we see in both experiments the conventional $s\bar{s}$ spin two resonance, the $f_2(1500)$, but the $f_J(1700)$ is missing in the LASS result. This would indicate that the $f_J(1700)$ is not an $s\bar{s}$ state.

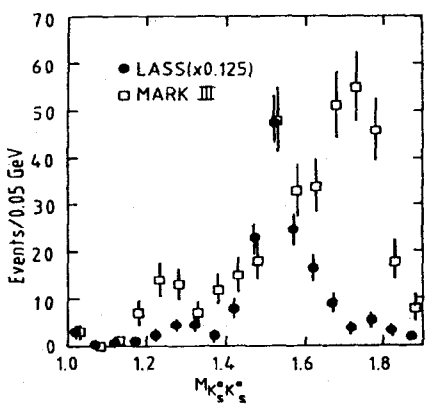

Figure 27. Comparison of KK mass distributions between Mark III and LASS.

From the BNL experiment studying the reaction $\pi^- p \rightarrow n\, K_s K_s$ at 23 GeV incident pion momentum, a scalar signal was claimed at 1730 MeV. There is an excess of events in the scalar wave intensity at 1.7 GeV as shown in Figure 28. This signal was attributed to a radial excitation [called the S^*'(1770) in their paper] of the $f_o(980)$ which was seen in this reaction at BNL but not in radiative J/ψ decays. A mass and width of 1771^{+11}_{-53} MeV and 200^{+156}_{-9} MeV was obtained.[32]

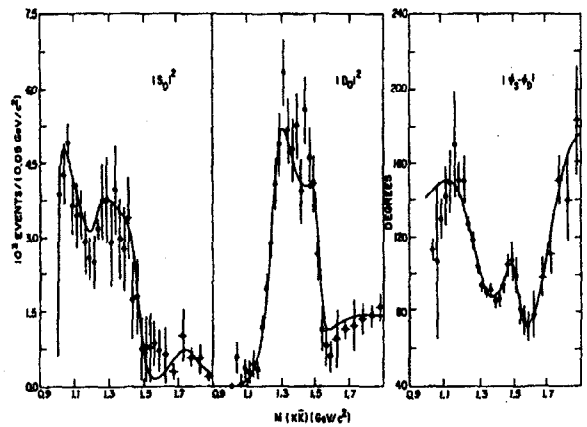

Figure 28. Partial wave analysis results from BNL.[33]

The WA76 experiment studies the reaction $pp \rightarrow p_f\,(KK)\,p_s$. In this reaction, centrally produced resonances may be coupled to gluons. In Figure 29 is the $K_s K_s$ mass plot from WA76 showing a clear $f_2(1500)$ signal and events at 1700 MeV. A fit of this signal yielded m = 1748 ± 10 MeV and Γ = 264 ± 25. A WA76 spin-parity study[34] prefers spin two for the resonance.

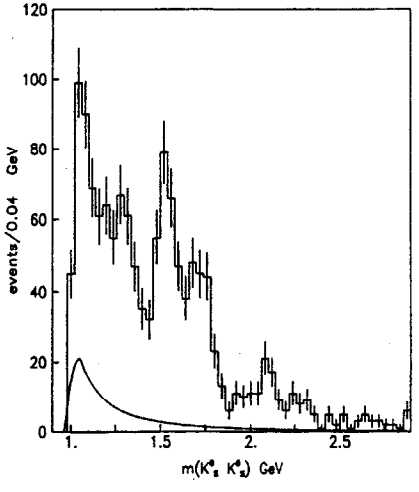

Figure 29. K_sK_s mass from WA76 (Ref. 35).

6.3 Spin-Parity Analysis

The spin-parity test of the *KK* signal in the radiative *J*/ψ data has been performed on the Mark III and BES data. The analysis of the *KK* signal is complicated due to the overlapping tensor and scalar signals and also due to the backgrounds from other channels such as $J/\psi \rightarrow K^*K$. In Figure 30 is a Dalitz plot of the mass squared of γK^+ versus γK^- and γK_s versus γK_s from the reaction $J/\psi \rightarrow \gamma K^+K^-$ and γK_SK_S. In the K^+K^- plot, there are backgrounds from K^*K which appear as bands (vertical and horizontal) near $m^2 = 0.5$ GeV^2.

A proper analysis of this complex channel required a moment analysis. Below in Figure 31 are the decay angles for a *J*/ψ radiative decay into two pseudoscalars. In this case, there are two sets of angles and this will require a set of double moments.

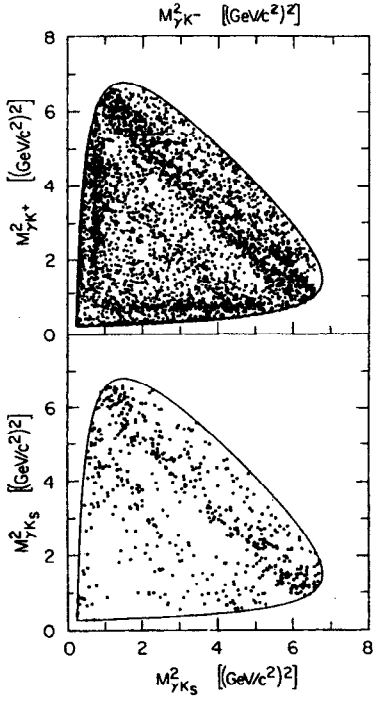

Figure 30. Dalitz plot $J/\psi \rightarrow \gamma KK$ and γK_sK_s from Mark III.

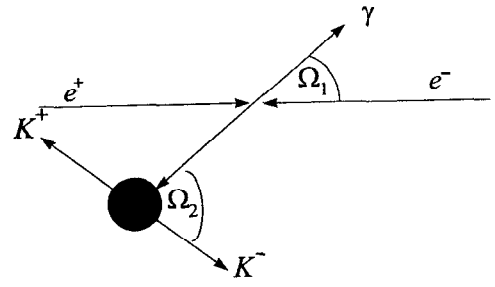

Figure 31. Schematic diagram of $ee \to J/\psi \to X, X \to KK$.

The Mark III data[36] is for the K_sK_s, K^+K^-, and $\pi^+\pi^-$ channels are shown in Figure 32. After fitting the moments, the amplitudes are extracted and the intensities for the scalar and tensor decay are derived which are plotted for the three channels in Figure 32 and Figure 33.

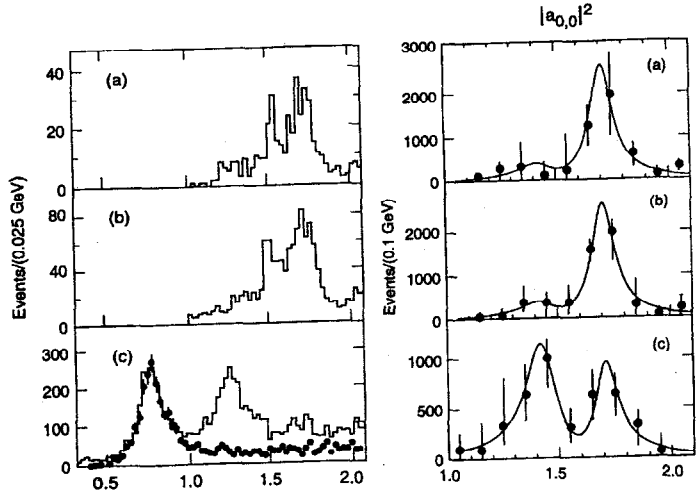

Figure 32. Mass distributions in GeV (left) and scalar intensities (right) of (a) K_sK_s, (b) K^+K^-, and (c) $\pi^+\pi^-$.

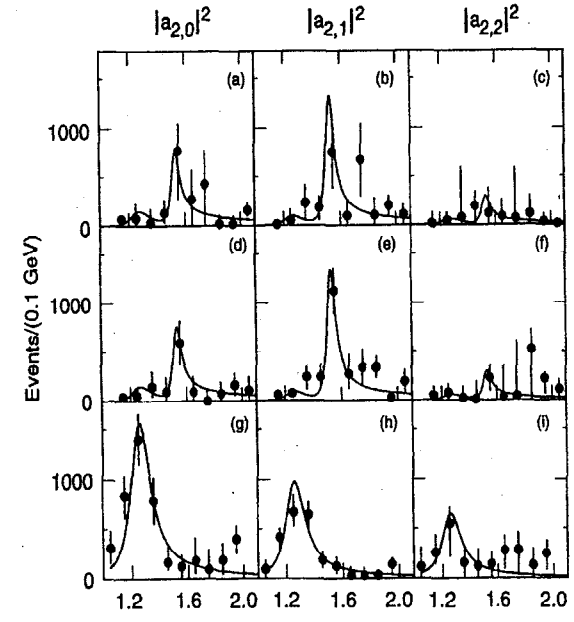

Figure 33. Tensor intensities for helicities 0,1,2 for (a)–(c) K_sK_s, (d)–(f) K^+K^-, and (g)–(i) $\pi^+\pi^-$ from Mark III.

The intensity of the different channels reveal the following:

- $f_2(1270)$ in the tensor $\pi\pi$ channel
- $f_2(1500)$ in the tensor K^+K^- and K_sK_s channels
- $f_J(1700)$ in the scalar $\pi\pi$, K^+K^-, and K_sK_s channels
- a signal at ~1400 MeV in the scalar $\pi\pi$ channel.

The conventional $f_2(1270)$ and $f_2(1500)$ mesons appear in the correct channel. The $f_J(1700)$ is found to be scalar, although there is nonzero spin two intensity in the 1700 MeV region. There is a scalar $\pi\pi$ signal ~1400 MeV which may be related

to the Crystal Barrel signal which was identified at 1330 MeV with a broad Γ = 760 MeV width. The $f_0(1500)$ is not observed.

Signal	Mass (MeV)	Width (MeV)	BR (10^{-4})
$f_0(1430)$	1429^{+43}_{-37}	169^{+111}_{-76}	$4.3^{+2.7}_{-1.7}$
$f_1(1700)$	1704^{+16}_{-23}	124^{+52}_{-44}	$9.5^{+2.5}_{-2.0}$

Table 7. Results of K_sK_s, K^+K^-, and $\pi\pi$ fits from Mark III.

Additional evidence for a scalar signal is provided by certain linear combinations of moments which contain only scalar amplitudes. These are plotted in Figure 34 and demonstrate consistency in the analysis procedure.

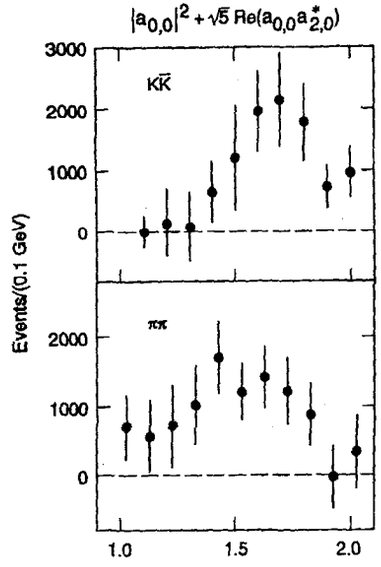

Figure 34. Scalar linear combinations of moments for K_sK_s and K^+K^- from the Mark III.

The BES group has recently published a moment analysis of the K^+K^- channel. The results of the scalar intensity are shown in Figure 35. There is a clear excess of scalar intensity near 1.8 GeV. However, the results of the tensor fit indicate an $f_2(1500)$ signal and a large tensor signal at 1700 MeV in disagreement with the Mark III results. The BES results are listed in Table 8.

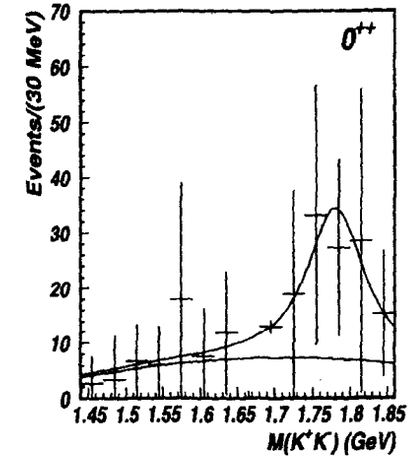

Figure 35. KK scalar wave intensity from BES.[37]

Spin	Mass (MeV)	Width (MeV)	BR (10^{-4})
scalar	$1781 \pm 8^{+10}_{-31}$	$85 \pm 25^{+22}_{-19}$	$0.8 \pm 0.1^{+0.3}_{-0.1}$
tensor	$1696 \pm 5^{+9}_{-34}$	$103 \pm 18^{+30}_{-11}$	$2.5 \pm 0.4^{+0.9}_{-0.4}$
$f_2(1525)$	$1516 \pm 5^{+9}_{-15}$	$60 \pm 23^{+13}_{-20}$	$1.6 \pm 0.2^{+0.6}_{-0.2}$

Table 8. Results of fits to KK analysis from BES.

6.4 $f_J(1700)$ Summary

The $f_J(1700)$ results include:

- production in radiative J/ψ and central production
- scalar spin in radiative J/ψ decays
- decay modes KK, $\eta\eta$, $\pi\pi$
- KK decays appear in recoil of $J/\psi \rightarrow \omega KK$.
- approximate SU(3) flavor singlet behavior, favors KK.

6.5 $\xi(2.2)$ Evidence

Evidence for the $\xi(2.2)$, a narrow resonance with a mass near 2.2 GeV observed in radiative J/ψ decays and decaying into K^+K^- and K_sK_s, was first obtained by Mark III[38] in 1985. Subsequently, the DM2[39] did not find the $\xi(2.2)$, but a broad signal in the 2.2 GeV region and concluded that the Mark III evidence may have been a fluctuation. Later evidence of a 2.2 GeV signal in K_sK_s and $\eta\eta'$ has been reported from the LASS[40] and GAMS[41] groups.

Recently, the BES group[37] reported evidence for the $\xi(2.2)$ in K^+K^-, K_sK_s, $\pi^+\pi^-$, and $p\bar{p}$. This new evidence of nonstrange decay modes appears to provide evidence that the $\xi(2.2)$ is more flavor symmetric.

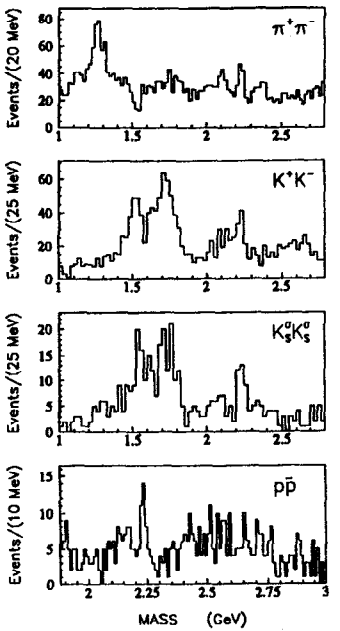

Figure 36. $J/\psi \rightarrow \gamma\pi\pi$, γK^+K^-, γK_sK_s, γpp from BES.[42]

New evidence[43] for the $\xi(2.2)$ comes from preliminary results from the L experiment at LEP. In the gluon jet, which is the least energetic jet in a three-je decay of the Z^0, an excess of events in K_sK_s are observed at $M = 2.234$ GeV. I the more energetic jets, which are expected to be the quark jets, the signal i absent.

7. Study of D_s Decays

The study of hadronic physics in the weak decays of charm mesons provide a new and possibly clean method to study mesons. This is now possible due to the high statistics data from charm fixed-target experiments. From the E791 experiment comes a clean $f_0(980)$ signal from the weak D_s decays. Figure 37 is the 3π mass where charged D and D_s signals are observed from the E791 group.

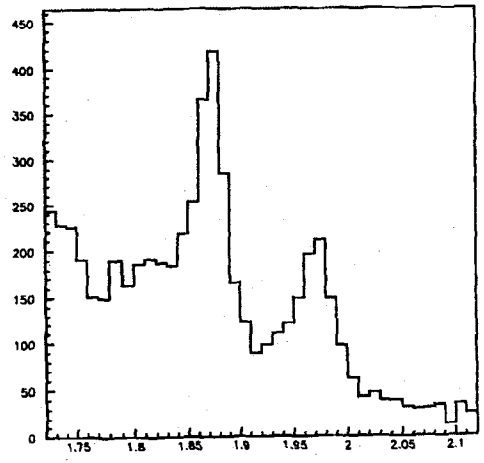

Figure 37. 3π mass from E791 (Ref. 44).

Restricting to the events at the D_s mass, the $\pi^+\pi^-$ mass squared is plotted in Figure 38. A clear peak is seen near 1 GeV which is most likely the $f_0(980)$. A broader peak is seen at m^2 = 1.9 GeV^2 (m = 1.35 GeV) which may be related to the 1.4 GeV resonance seen by the Crystal Barrel. No evidence is seen for the $f_0(1500)$ which would appear at $m^2 = 2.25$ GeV^2 in the figure.

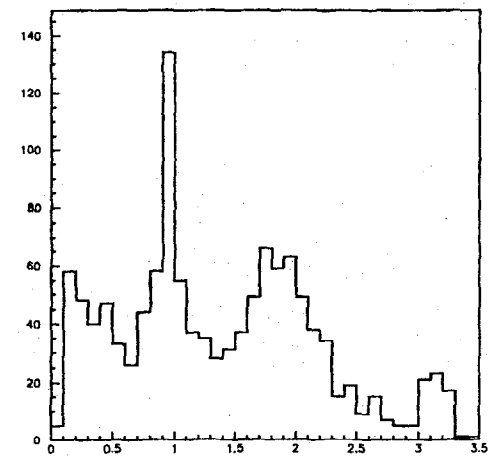

Figure 38. Mass $\pi^+\pi^-$ squared from experiment E791.

In Figure 39 is a folded Dalitz plot of the decay $D_s \rightarrow 3\pi$. Where the $f_0(980)$ overlaps at 1 GeV^2, there is a constructive interference. There are also enhancements at low $\pi\pi$ mass below 0.5 GeV and near $m^2 = 2$ GeV^2.

The $\pi\pi$ mass distribution is very similar to the one produced in $J/\psi \rightarrow \phi\pi\pi$, in Figure 6, where we expect the $\pi\pi$ states to couple to $s\bar{s}$. The D_s weak decay should also produce a recoiling $s\bar{s}$ quark pair. Hence, the $\pi\pi$ recoil should be very similar to the $\pi\pi$ recoil in $J/\psi \rightarrow \phi\pi\pi$. This provides qualitative agreement between the quark content produced in the OZI decay of the J/ψ and the weak decay of the D_s.

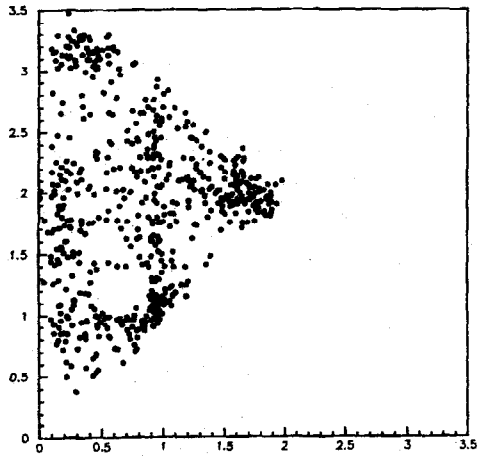

Figure 39. Dalitz plot of $\pi^+\pi^-$ vs $\pi^+\pi^-$ from E791.

Since we find that the $f_o(980)$ and possibly other higher $\pi\pi$ states are visible in the D_s, it is likely the KK mass from $J/\psi \rightarrow \phi KK$, will be similar to the KK mass in $D_s \rightarrow \pi KK$. This information may be useful to isolate the $D_s \rightarrow \phi\pi$ contributions from $KK\pi$ and to correct the absolute D_s branching ratios.

8. Search for Exotic States

The most promising candidate for an exotic state has been evidence of a resonance decaying into $\eta\pi$ in a P wave with a mass near ~1.3 GeV. Such a state would have $J^{PC} = 1^{-+}$.

The first evidence came from the GAMS experiment[45] which studied the reaction, $\pi^- p \rightarrow nX$, $X \rightarrow \eta\pi^0$ with incident pion momentum of 100 GeV. A partial wave analysis indicated a forward-backward asymmetry between a P wave signal and the D wave from the nearby $a_2(1320)$. The P wave signal had a mass and width of 1406 ± 20 MeV and 180 ± 30 MeV.

Another experiment from the BENKEI group[46] at KEK, studied the reaction $\pi^- p \rightarrow pX$, $X \rightarrow \eta\pi^+$ at 6.3 GeV incident pion momentum. A clear P wave signal near the a_2 at 1325 ± 5 MeV with a width of 126 ± 14 MeV was observed. In Figure 40 is shown the results from the BENKEI experiment. The upper plot is the D wave intensity of the a_2 resonance. The middle plot is the P wave signal showing a clear excess at the same place as the a_2. The lower plot is the phase variation between the P wave and the D wave where the D wave signal is assumed to be constant. Apparently, there is no phase variation seen between the P and D waves.

A new experiment at BNL has also studied this reaction, and this will be reported at the topical conference of this meeting by N. Cason.[2]

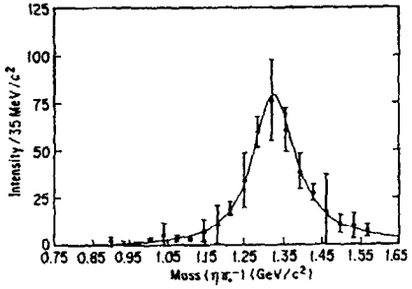

Fitting of the Breit-Wigner formula to the D_+ wave.

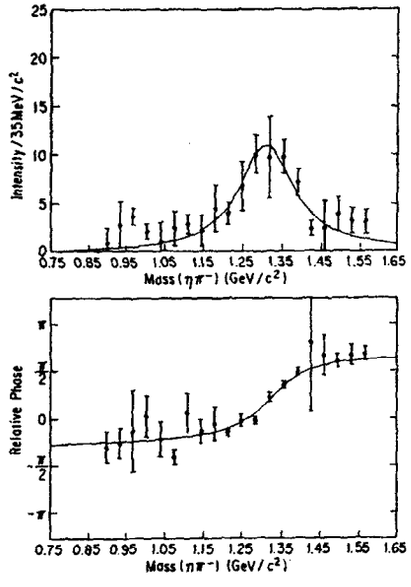

Figure 40. Partial wave results on ηπ from BENKEI.[46]

9. Summary and Outlook

The $f_o(1500)$ and $f_J(1700)$ resonances are strong glueball candidates. However, more experimental work will be very important to consolidate and confirm the evidence.

For the $f_o(1500)$, the search for non-$p\bar{p}$ production and a $K\bar{K}$ decay mode will be very important. In the future, more BES data on J/ψ decays may reveal $f_o(1500)$ evidence in 4π and 2π decays. Also, high statistics hadronic searches at BNL may add new information. Unfortunately, LEAR is no longer running, so the only hope for more $p\bar{p}$ data is from the E760 group which will still be running for charmonium physics. Perhaps they can confirm the scalar spin and find a KK decay mode.

For the $f_J(1700)$, new data will be available from BES in J/ψ decays. Much higher statistics are required for convincing spin-parity tests. Also, the $\pi\pi$ decay modes and the hadronic production of the $f_J(1700)$ require confirming measurements.

In the future, the B factories and charm experiments (E835) will provide more charm data. The weak semileptonic D_s and D decays may add much needed evidence for scalars.

REFERENCES

[1] M. Doser, these proceedings.

[2] N. Cason, these proceedings.

[3] *Hadron '95, 6th Int. Conf. On Hadron Spectroscopy*, Manchester, UK, July 10-14, 1995, edited by. M. Birse, G. Lafferty, and J. McGovern.

[4] L. Kopke and N. Wermes, Physics Reports **174**, 67 (1989).

[5] M. Chanowitz, SLAC Summer School Lectures, July 27-29, 1981.

[6] Particle Data Group, Phys. Rev. D **54**, 1 (1996).

[7] F. Close, *An Introduction to Quarks and Partons* (Academic Press, 1979).

[8] Physics of Atomic Nuclei, **57**, 1465 (1994), edited by Y. Kalashnikova, L. Kondratyuk, A. Kudryavtsev, and N. Smorodinskaya.

[9] See the talk by Thomas DeGrand in these proceedings.

[10] For a treatment of the quark model see Ref. 7.

[11] J. Weinstein, Phys. Rev. D **27**,588 (1983).

[12] See the introductory treatment by W. Burcham and M. Jobes, *Nuclear and Particle Physics* (Longman Scientific & Technical, 1995).

[13] J. D. Jackson, *Classical Electrodynamics* (Wiley, New York, 1975).

[14] S. Flatte, Phys. Lett. B **63**, 224 (1976).

[15] J. Richman, *An Experimentalist's Guide to the Helicity Formalism*, CALT-60-1148, June 1984.

[16] H. Pilkuhn, *The Interactions of Hadrons* (North-Holland Publishing, 1967).
For an application of this technique, see R. Longacre, T. Lasinski, R. Rosenfeld, G. Smadja, D. Leith, and R. Cashmore, Phys. Rev. D **17**, 1795 (1978).

[17] T. Lasinski and R. Levi-Setti, *Strongly Interacting Particles*, (University of Chicago Press, 1973).

[18] L. Gray *et al.*, Phys. Rev. D **27**, 307 (1983).

[19] A. Adamo *et al.*, Phys. Lett. B **287**, 368 (1992).

[20] C. Amsler *et al.*, Phys. Lett. B **342**, 433 (1995).

[21] C. Amsler *et al.*, Phys. Lett. B **353**, 571 (1995).

[22] M. Abul Hasal in, *Hadron '95 Proceedings*, July 10-14, 1995, Manchester, UK, edited by M. Birse, G. Lafferty, and J. McGovern.

[23] D. Bisello *et al.*, contributed paper to the 1987 Int. Lepton and Photon Meeting, Hamburg, July 1987.

[24] D. Bugg *et al.*, Phys. Lett. B **353**, 378 (1995).

[25] Roger Lee, Ph.D thesis, Stanford University, SLAC-Report 282, 1985.

[26] See C. Amsler and F. Close, Phys. Lett. B **353**, 385 (1995).

[27] C. Dover *et al.*, Nucl. Phys. **43**, 379 (1991).

[28] T. Kalogeropoulos *et al.*, Phys. Rev. D **24**, 1759 (1981).

[29] M. Franklin, preprint SLAC-254, 1982.

[30] C. Edwards *et al.*, Phys. Rev. Lett. **48**, 458 (1982).

[31] R. Baltrusaitus *et al.*, Phys. Rev. D **35**, 2077 (1987).

[32] A. Etkin *et al.*, Phys. Rev. D **25**, 1786 (1982)

[33] A. Etkin *et al.*, Phys. Rev. D **25**, 1786 (1982); A. Etkin *et al.*, Phys. Rev. D **25**, 2446 (1982).

[34] T. Armstrong *et al.*, Phys. Lett. B **227**,186 (1989).

[35] T. A. Armstrong *et al.*, Z. Phys. C **51**, 351(1991).

[36] This analysis is from L. Chen's Ph.D. thesis, University of Vanderbilt. The fits in this review have been performed by W. Dunwoodie on the moments from L. Chen's thesis.

[37] J. Z. Bai *et al.*, Phys. Rev. Lett. **77**, 3959 (1996).

[38] R. Baltrusaitis *et al.*, Phys. Rev. Lett. **56**, 107 (1986)

[39] J. Augustin *et al.*, Phys. Rev. Lett. **60**, 2238 (1988)

[40] D. Aston *et al.*, Phys. Lett. B **215**, 199 (1988)

[41] D. Alde *et al.*, Phys. Lett. B **177**, 120 (1986)

[42] J. Z. Bai *et al.*, Phys. Rev. Lett. **76**, 3502 (1996).

[43] G. Forconi, DPF96, Minnesota, Minn., August 1996.

[44] Preliminary results from M. Sokoloff.

[45] D. Alde *et al.*, Phys. Lett. B **205**, 205 (1988).

[46] H. Aoygi *et al.*, Nuovo Cimento A **107**, 1925 (1994).